Science Arts & Métiers (SAM)

is an open access repository that collects the work of Arts et Métiers Institute of Technology researchers and makes it freely available over the web where possible.

This is an author-deposited version published in: https://sam.ensam.eu
Handle ID: .http://hdl.handle.net/10985/10098

To cite this version :

Boris PIOTROWSKI, Tarak BEN ZINEB, Etienne PATOOR, André EBERHARDT - Modeling of niobium precipitates effect on the Ni 47Ti 44Nb 9 Shape Memory Alloy behavior - International Journal of Plasticity - Vol. 36, p.130-147 - 2012

Any correspondence concerning this service should be sent to the repository Administrator : scienceouverte@ensam.eu

Arts et Métiers Institute of Technology

ACCEPTED MANUSCRIPT

Modeling of niobium precipitates effect on the $Ni_{47}Ti_{44}Nb_9$ Shape Memory Alloy behavior

B. Piotrowski[a,b,c], T. Ben Zineb[a], E. Patoor[b], A. Eberhardt[b]

[a] *Laboratoire d'Energtique et de Mecanique Theorique et Appliquee (LEMTA), Lorraine University, CNRS, 2 rue Jean Lamour; 54500 Vandoeuvre-les-Nancy, France*
[b] *Laboratoire d'Etude des Microstructures et de Mécanique des Matériaux (LEM3), Lorraine University, Arts et Métiers ParisTech, ENIM, CNRS, Ile du Saulcy; 57045 Metz cedex 01, France*
[c] *Etudes et Productions Schlumberger, 1 rue Henri Becquerel, 92140, Clamart France*

Abstract

Commercial $Ni_{47}Ti_{44}Nb_9$ Shape Memory Alloy (SMA) is generally adopted for tightening applications thanks to its wide transformation hysteresis, compared with classical NiTi. Its sensibility to thermo-mechanical treatments allows it to be either martensitic or austenitic in a wide range of temperature, between -60 °C and 80 °C. A modeling of niobium precipitates effects on $Ni_{47}Ti_{44}Nb_9$ SMA behavior is proposed. For this object, a two phases thermo-mechanical model is developed. It describes the global effective behavior of an elastoplastic inclusion (niobium precipitates) embedded within a SMA matrix. The constitutive law developed by Peultier et al. [Peultier, B. et al., 2006] and improved by Chemisky et al. [Chemisky, Y. et al., 2011] is adopted to model the matrix shape memory behavior. The elastoplastic constitutive law for inclusion is the one proposed by Wilkins with Simo and

Email addresses: boris.piotrowski@metz.ensam.fr (B. Piotrowski), tarak.ben-zineb@univ-lorraine.fr (T. Ben Zineb), etienne.patoor@metz.ensam.fr (E. Patoor)

ACCEPTED MANUSCRIPT

Hughes's radial return algorithm. The Mori-Tanaka scale transition scheme is considered for the determination of the effective constitutive equations. Obtained results highlight the effect of niobium precipitates on the thermo-mechanical behavior of $Ni_{47}Ti_{44}Nb_9$, and particularly on the corresponding hysteresis size. It appears that the niobium plasticity increases this hysteresis size. The developed constitutive law has been implemented in the ABAQUS® Finite Element code and considered for the numerical prediction of the tightening pressure in a connection application.

Key words: Shape Memory Alloy, Modeling, Homogenization, Niobium precipitates, Martensite stabilization

1. Introduction

Since the 70's, research works continue to be carried out on four main Shape Memory Alloy families: copper-based, iron-based, NiMnGa-based and NiTi-based, in order to improve their performance. Nowadays, most of industrial applications are based on NiTi SMAs because they present excellent properties as large recovery force and good corrosion resistance. Moreover, their biocompatibility allows them to be used in medical field. The NiTi transformation temperature hysteresis is about 30 or 40 °C (Strnadel et al., 1995), which can by modified by element addition: copper decreases it (Nam, 1990), iron increases it until 70 °C (Harrison et al., 1973) and niobium until 160 °C (He and Rong, 2004). Zhang et al. (1991) show that niobium addition into NiTi induces precipitation of β-Nb particles. These precipitates exhibit a ductile elastoplastic behavior (Zhao et al., 1990). In $Ni_{47}Ti_{44}Nb_9$, as in other SMA, elastic strain energy is stored during martensitic transformation, due

ACCEPTED MANUSCRIPT

to incompatibilities between martensite domains (Zhang et al., 1990). During a mechanical treatment called "predeformation", niobium precipitates are assumed to relax this elastic energy (Piao et al., 1993). The consequence is the increase of reverse transformation temperatures, which allows a larger field of industrial applications.

To design $Ni_{47}Ti_{44}Nb_9$ applications by Finite Element Method, the behavior of this alloy has to be modeled. In this study, $Ni_{47}Ti_{44}Nb_9$ is considered as a composite with shape memory matrix and niobium elastoplastic inclusions. However, due to this complex microstructure, there is currently no model which accurately describes the specific behavior of this alloy.

Models were developed for classical SMA without elastoplastic precipitates. Two categories of model can be considered: micro-mechanical approaches and phenomenological ones. The first category is based on a 3D micro-mechanical description at the grain scale of the martensitic transformation (Patoor et al., 1996; Huang and Brinson, 1998; Gao et al., 2000; Patoor et al., 2006; Peng et al., 2008). These models contain many internal variables describing accurately martensite variants activation and reorientation, and some of them describe interaction between martensitic transformation and plastic deformation during interface propagation (Idesman and Stein, 2000; Levitas, 2002; Bartel et al., 2011). However, they are inappropriate for computation with finite element method. Macroscopic phenomenological models involve a limited set of two or three macroscopic internal variables as self-accommodated and oriented martensite (Panico and Brinson, 2007; Popov and Lagoudas, 2007; Thiebaud et al., 2007), mass fraction of martensite (Muller and Bruhns, 2006), martensite volume fraction and mean trans-

ACCEPTED MANUSCRIPT

formation strain (Peultier et al., 2006; Zaki and Moumni, 2007), martensite volume fraction, mean transformation strain, self-accommodated martensite volume fraction, mean strain due to inelastic accommodation of twins inside martensite (Chemisky et al., 2011), transformation strain and permanent inelastic strain (Auricchio et al., 2007). These models well describe the effect of the martensitic transformation without plastic strain consideration. Other models adapted to iron-Based SMA (Goliboroda et al., 1999; Jemal et al., 2009; Khalil et al., 2012) or TRIP Steels (Cherkaoui et al., 1998; Fischer et al., 2000; Petit et al., 2007; Kouznetsova and Geers, 2008) describe the effects of transformation and plastic strain and their interaction on the thermo-mechanical behaviour. This consideration leads to a well description of cyclic loadings (Feng and Sun, 2007; Kan and Kang, 2010). Viscoplastic strains in a SMA material have been taken into account by Hartl et al. (2010) who have proposed a three-dimensional constitutive model adapted to high temperatures.

For $Ni_{47}Ti_{44}Nb_9$, martensitic transformation is only observed into NiTi matrix. Plastic strain occurs in the ductile niobium inclusions, and the alloy has to be modeled as a SMA composite. Many models consider the case of SMA composites, using SMA wires or ribbons embedded in an elastic matrix. The composite can act with an active or passive way depending on the application. For active applications, it has been shown that SMA wires can act as internal stress generators in polymer composite systems (Bollas et al., 2007), which induce the SMA activation. Some SMA composites models are developed for structure morphing (Brinson et al., 1997; Oh et al., 2001; Armstrong and Lorentzen, 2001; Chemisky et al., 2009a), or for vibration control

ACCEPTED MANUSCRIPT

(Brinson and Lammering, 1993; Aoki and Shimamoto, 2003; Zhang et al., 2007). Other ones simulate the passive behavior to control some properties of the composite, as stiffness (Boyd and Lagoudas, 1996), hysteresis properties after cycling (Kawai, 2000) or the overall behavior (Cherkaoui et al., 2000). The impact of the shape of the inclusions on the effective composites properties has also been studied (Lu and Weng, 2000). However, few models describe the behavior of SMA composites whose inclusions are embedded in a SMA matrix. Several kinds of inclusions have to be considered. These inclusions can be voids like in porous Shape Memory Alloys. They are developed for biomedical applications. Constitutive models describing such behavior are proposed by Panico and Brinson (2008), and Entchev and Lagoudas (2002). Inclusions can also have elastic behavior, as Zirconium in Copper based SMAs (Collard et al., 2008) and Ni_4Ti_3 in NiTi (Chemisky et al., 2009b).

In order to take into account the micro-heterogeneous character of $Ni_{47}Ti_{44}Nb_9$ and describe the effective macroscopic constitutive law of composite materials, scale transition techniques are adopted. We consider the problem of an inclusion embedded into an infinite homogeneous medium (Eshelby, 1961). When the matrix can be clearly identified in the composite, its behavior is adopted for the reference medium, which consists of Mori-Tanaka scheme (Mori and Tanaka, 1973). Nevertheless, for materials with non-linear behavior, Eshelby problem has no exact analytical solution and a linearization is needed. An approximated solution based on Eshelby one is also generally used, especially in elastoplasticity (Kroner, 1961; Hill, 1965; Berveiller and Zaoui, 1979) and viscoplasticity (Hutchinson, 1976; Mercier and Molinari,

ACCEPTED MANUSCRIPT

2009). Due to specific micro-heterogeneous character of $Ni_{47}Ti_{44}Nb_9$ (Zhang et al., 1991), Mori-Tanaka mean field approach is adopted in this work to predict the effective behavior. Such approach is widely applied to conventional materials where the inelastic strain in matrix or inclusions is induced by plastic deformation or damage (Meraghni and Benzeggagh, 1995; Desrumaux et al., 2001; Boudifa et al., 2009).

In this paper, it is proposed to extend this approach for SMA materials where the inelastic strain is induced by phase transformation and plastic strain. This work is focused on the behavior modeling of ductile elastoplastic inclusions embedded in a SMA matrix, based on micromechanical approach using the Mori-Tanaka scale transition technique. In particular, the effective behavior of $Ni_{47}Ti_{44}Nb_9$ has been investigated. This model has been implemented in the ABAQUS® Finite Element code via the subroutine UMAT (User MATerial). The first part presents the $Ni_{47}Ti_{44}Nb_9$ proposed model, divided into three subsections: SMA matrix behavior modeling, elastoplastic inclusion behavior modeling and homogenization leading to an effective constitutive law. The Duval-Chemisky model (Chemisky et al., 2011) is chosen for the SMA matrix behavior modeling due to its robustness and its fine behavior description of NiTi alloys for complex loadings (tension, torsion, partial loadings, recovery strain at constant stress and recovery stress at constant strain). In addition, this model is already implemented in a FE code and has been successfully validated with experimental data. A phenomenological constitutive model of plasticity is adopted (Simo and Hughes, 1998) to describe inclusion behavior. The development which leads, from constitutive equations inside matrix and inclusions, to effective behavior law is presented

ACCEPTED MANUSCRIPT

in the end of this part. The following one deals with numerical resolution of the non-linear constitutive equations. The homogenization strategy taking into account phase transformation in matrix and plastic strain in inclusions via Mori-Tanaka scheme is presented. Eventually, numerical results are discussed and the effects of plastic strain in niobium precipitates on the transformation properties of the composite are investigated.

2. Effective behavior modeling: constitutive law

In this part, the modeling strategy adopted to describe the $Ni_{47}Ti_{44}Nb_9$ behavior is exposed. The general case of a composite with elastoplastic inclusions embedded into a shape memory matrix is considered.

2.1. RVE and homogenization strategy

In order to model the thermo-mechanical behavior of NiTiNb alloy, a Representative Volume Element (RVE) has to be defined. This RVE depends on both $Ni_{47}Ti_{44}Nb_9$ microstructure and the adopted homogenization technique. Consequently, some microscopic observations by SEM are conducted. Micrographs in Figure 1 show the microstructure of the alloy in two perpendicular planes, which allows to build the 3D microstructure.

ACCEPTED MANUSCRIPT

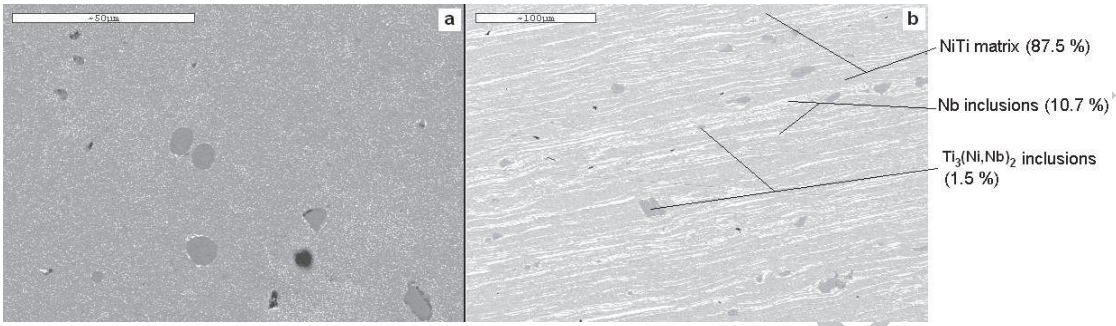

Figure 1: Micrographs in the precipitates longitudinal direction (a) and transverse one (b).

Three phases are highlighted. The first one is the matrix, which appears in low grey in micrographs, and which corresponds to a NiTi shape memory alloy. Image analysis shows that the surface fraction of this phase is about 87.5 %, and chemical analyses shows that matrix composition is near to 51 at.% Ni and 49 at.% Ti. The second one is composed of long white ellipsoidal inclusions, which correspond to the Nb-rich phase and whose surface fraction is about 10.7 %. The last one is composed of high grey particles. A SEM analysis shows that it corresponds to $Ti_3(Ni,Nb)_2$ inclusions, as observed by Zhang et al. (1991). An image analysis reveals that these Ti-rich inclusions represent 1.5 % of surface fraction.

These observations show that a matrix phase mainly composed of NiTi is clearly identified, and Nb-rich inclusions are in a relatively low volume fraction, and well distributed. Few $Ti_3(Ni,Nb)_2$ particles are present in this alloy. Moreover, $Ti_3(Ni,Nb)_2$ inclusions are most of the time embedded by very ductile Nb-rich phase, so influence of these precipitates on the macroscopic behavior appears negligible and they are not considered in this model.

ACCEPTED MANUSCRIPT

Accordingly, the Mori-Tanaka scheme is adopted and the matrix material is chosen for the reference medium, in order to lead to the effective behavior. The RVE has consequently to be composed of SMA Matrix (NiTi) with elastoplastic inclusions (niobium). Inclusions are modeled with a spherical shape, further investigations will be conducted with ellipsoidal shape.
In order to lead to the effective thermo-mechanical constitutive law, the polycrystalline aggregate of NiTi matrix is described with a macroscopic model developed by Peultier et al. (2006), and improved by Chemisky et al. (2011). This 3D model is chosen for its ability to accurately describe the main SMA physical phenomena, both of tension/compression asymmetry for saturation of transformation strain, critical stress, hysteresis, and internal loops for superelastic and thermal cycles. Moreover, the material parameters of this model are representative of specific physical properties, and are easy to identify. Inclusions behavior is assumed to be elastoplastic, described by a power law, and an algorithm for plasticity is adopted (Wilkins, 1964; Simo and Hughes, 1998). The RVE effective behavior is obtained by a Mori-Tanaka scale transition technique starting from matrix and inclusion behaviors. In the next subsections, the adopted constitutive models for matrix and inclusions are detailed. Then the homogenization procedure is developed.

2.2. Thermo-mechanical constitutive law for SMA matrix

This part is a brief review of the SMA model considered in this work. It presents four internal variables: the martensite volume fraction f, the mean transformation strain $\bar{\varepsilon}_{ij}^{T}$ (Peultier et al., 2006), the mean twin accommodation strain $\bar{\varepsilon}_{ij}^{tw}$ and the volume fraction of twinned martensite f^{FA} (Chemisky

ACCEPTED MANUSCRIPT

et al., 2011). These variables are defined as follows:

$$f = \frac{V_M}{V} \tag{1}$$

$$\bar{\varepsilon}_{ij}^{T} = \frac{1}{V_M} \int_{V_M} \varepsilon_{ij}^{T} dV \tag{2}$$

$$\bar{\varepsilon}_{ij}^{tw} = \frac{1}{V_M} \int_{V_M} \varepsilon_{ij}^{tw} dV \tag{3}$$

$$f^{FA} = \frac{V^{tm}}{V_M} \tag{4}$$

V_M is the volume of martensite in the RVE, V is the RVE volume, ε_{ij}^{T} is the transformation strain tensor, ε_{ij}^{tw} is the local twin accommodation strain tensor and V^{tm} the volume of twinned martensite. Total strain in matrix is composed of several strains contributions describing physical mechanisms:

$$\varepsilon_{ij}^{tot} = \varepsilon_{ij}^{e} + \varepsilon_{ij}^{th} + \varepsilon_{ij}^{T} + \varepsilon_{ij}^{tw} \tag{5}$$

- the elastic strain ε_{ij}^{e},
- the thermal expansion strain ε_{ij}^{th},
- the transformation strain ε_{ij}^{T}, a product between the martensite volume fraction f and the mean transformation strain $\bar{\varepsilon}_{ij}^{T}$ ($\varepsilon_{ij}^{T} = f\bar{\varepsilon}_{ij}^{T}$).
- the twin accommodation strain ε_{ij}^{tw}, a product between the twinned martensite volume fraction f^{FA} and the mean twin accommodation strain $\bar{\varepsilon}_{ij}^{tw}$ ($\varepsilon_{ij}^{tw} = f^{FA}\bar{\varepsilon}_{ij}^{tw}$).

ACCEPTED MANUSCRIPT

A thermodynamic potential is assumed to model polycrystalline shape memory alloy (6). It corresponds to a macroscopic expression of the Gibbs free energy variation between an initial austenitic state and a biphasic Martensite-Austenite current one.

$$\begin{aligned}\Delta G(\sigma_{ij}^M, T, f, \bar{\varepsilon}_{ij}^T, f^{FA}, \bar{\varepsilon}_{ij}^{tw}) = &-\frac{1}{2}\sigma_{ij}^M S_{ijkl}^M \sigma_{kl}^M - \sigma_{ij}\alpha_{ij}^M \Delta T - \Delta T S^A - \sigma_{ij}^M f \bar{\varepsilon}_{ij}^T - \sigma_{ij}^M f^{FA}\bar{\varepsilon}_{ij}^{tw} \\ &+B(T-T_0)f + \frac{1}{2}f H_\varepsilon \bar{\varepsilon}_{ij}^T \bar{\varepsilon}_{ij}^T + \frac{1}{2}H_f f^2 + \frac{1}{2}f^{FA} H_{twin}\bar{\varepsilon}_{ij}^{tw}\bar{\varepsilon}_{ij}^{tw}\end{aligned} \tag{6}$$

T and σ_{ij}^M are respectively the temperature and the Cauchy stress tensor in matrix.

S_{ijkl}^M, α_{ij}^M, B, S^A, T_0 are respectively the matrix compliance tensor, the matrix thermal expansion tensor, the parameter describing transformation temperatures variation with stress level, the austenitic entropy and the equilibrium temperature. H_ε, H_f are two parameters characterising in a global way incompatibilities between grains and between martensite variants. H_{twin} is a scalar twin accommodation parameter.

From this expression, thermodynamic forces (transformation, orientation, twin accommodation, entropic and elastic) associated to each variable are derived.

$$F_f = -\frac{\delta(\Delta G)}{\delta f} = \sigma_{ij}^M \bar{\varepsilon}_{ij}^T - B(T-T_0) - H_f f - \frac{1}{2}H_\varepsilon \bar{\varepsilon}_{ij}^T \bar{\varepsilon}_{ij}^T \tag{7}$$

$$fF_{\bar{\varepsilon}_{ij}^T} = -\frac{\delta(\Delta G)}{\delta \bar{\varepsilon}_{ij}^T} = f((\sigma_{ij}^D)^M - H_\varepsilon \bar{\varepsilon}_{ij}^T) \tag{8}$$

$$f^{FA}F_{\bar{\varepsilon}_{ij}^{tw}} = -\frac{\delta(\Delta G)}{\delta \bar{\varepsilon}_{ij}^{tw}} = f^{FA}((\sigma_{ij}^D)^M - H_{twin}\bar{\varepsilon}_{ij}^{tw}) \tag{9}$$

$$F_T = -\frac{\delta(\Delta G)}{\delta T} = \sigma_{ij}^M \alpha_{ij}^M + S^A - Bf \tag{10}$$

ACCEPTED MANUSCRIPT

$$F_{\sigma_{ij}^M} = -\frac{\delta(\Delta G)}{\delta \sigma_{ij}^M} = S_{ijkl}^M \sigma_{kl}^M + \alpha_{ij}^M \Delta T + f\bar{\varepsilon}_{ij}^T + f^{FA}\bar{\varepsilon}_{ij}^{tw} \tag{11}$$

$(\sigma_{ij}^D)^M$ is the deviatoric part of the matrix stress tensor $(\sigma_{ij}^D)^M = \sigma_{ij}^M - \delta_{ij}\frac{\sigma_{kk}^M}{3}$) with δ_{ij} the Kronecker symbol. These driving forces are compared with critical ones in order to determine the activated mechanisms. Then, by taking into account the consistency rule ($\dot{F}_x = \dot{F}_x^C$ with $x = f,\ \bar{\varepsilon}^T,\ T, \sigma_{ij}^M$), the constitutive law is derived in an incremental way as follows:

$$\dot{\sigma}_{ij}^M(r) = l_{ijkl}^M(r)\dot{\varepsilon}_{kl}^M(r) - m_{ij}^M \dot{T} \tag{12}$$

l^M and m^M are respectively the mechanical and thermal tangent operators. Further details about the description of specific behavior aspects as tension compression asymmetry, saturation, internal loops and hysteresis can be find in Chemisky et al. (2011)

2.3. Elastoplastic inclusion behavior

Inclusions have an elastoplastic behavior. An algorithm for plasticity developed by Simo and Hughes (1998) has been adopted to model the elastoplastic behavior, using the Von Mises yield condition based on a return mapping method, originally proposed by Wilkins (1964). The total strain in inclusion is decomposed as follows:

$$\varepsilon_{ij}^{tot} = \varepsilon_{ij}^e + \varepsilon_{ij}^{th} + \varepsilon_{ij}^p \tag{13}$$

with:

- the elastic strain ε_{ij}^e,
- the thermal expansion strain ε_{ij}^{th},

ACCEPTED MANUSCRIPT

- the plastic strain $\dot{\varepsilon}^p_{ij} = \sqrt{\frac{3}{2}}\dot{p}.\eta_{ij}$ with η_{ij} the flow direction ($n_{ij} = \frac{\delta f}{\delta \sigma_{ij}}$ and f is the yield surface) and p the cumulative plastic strain ($\dot{p} = \sqrt{\frac{2}{3}\dot{\varepsilon}^p_{ij}\dot{\varepsilon}^p_{ij}}$).

A Swift hardening law described by the Ludwick type yielding function is considered for an isotropic hardening:

$$\sigma_{eq} = \sigma_Y + H_{iso}p^{\frac{1}{n}} \tag{14}$$

σ_Y is the plastic yield stress, H_{iso} and n are two hardening parameters. The constitutive equation can be written as follows:

$$\dot{\sigma}^I_{ij}(r) = l^I_{ijkl}(r)\dot{\varepsilon}^I_{kl}(r) - c^I_{ijkl}(r)\alpha^I_{kl}\dot{T} \tag{15}$$

with l^I the elastoplastic tangent operator, α^I the thermal expansion tensor, and c^I the fourth order elastic tensor.

2.4. Mori-Tanaka homogenization: inelastic solution

$Ni_{47}Ti_{44}Nb_9$ is considered as a composite whose SMA matrix (NiTi) contains spherical elastoplastic inclusions (niobium precipitates). Mori-Tanaka scale transition technique induces macro-homogeneous constitutive law describing $Ni_{47}Ti_{44}Nb_9$ micro-heterogeneous behavior. The Eshelby solution which considers the general case of an inelastic inclusion placed in an inelastic matrix gives a relation between inclusion and macroscopic strains (16):

$$\dot{\varepsilon}^I_{mn} = A^{esh}_{mnij}\dot{E}_{ij} \tag{16}$$

with

$$A^{esh}_{mnij} = [I_{ijmn} - T^{II}_{ijkl}(l^M_{klmn} - l^I_{klmn})]^{-1} \tag{17}$$

ACCEPTED MANUSCRIPT

$T^{II}_{ijkl} = \int_V \Gamma_{ijkl}(r - r')dV'$ is the fourth order interaction tensor derived from Eshelby inclusion theory, which depends on inclusion geometry and matrix material. ^{I} and ^{M} superscripts denote respectively Inclusion and Matrix. In Mori-Tanaka scheme, strain rate applied to the boundary of inclusion is assumed equal to the strain rate in matrix (Mori and Tanaka, 1973).

$$\dot{\varepsilon}^I_{ij} = \dot{\varepsilon}^M_{ij} + T^{II}_{ijkl}(l^M_{klmn} - l^I_{klmn})\dot{\varepsilon}^I_{mn} \tag{18}$$

Moreover, the global strain rate is assumed equal to the sum between inclusion strain rate and matrix strain rate, weighted by their volume fractions. The inclusion volume fraction is denoted z, and consequently the matrix one is $(1 - z)$ (with $0 < z < 1$).

$$\dot{E}_{ij} = z\dot{\varepsilon}^I_{ij} + (1 - z)\dot{\varepsilon}^M_{ij} \tag{19}$$

The fourth order concentration tensor is derived from equations (18) and (19), and strain inside matrix and inclusion can also be determined starting from macroscopic one as follows:

$$\begin{aligned} \dot{\varepsilon}^I_{mn} &= A^{MT}_{mnij}\dot{E}_{ij} \\ \dot{\varepsilon}^M_{mn} &= \frac{1}{1-z}(I_{mnij} - zA^{MT}_{mnij})\dot{E}_{ij} \end{aligned} \tag{20}$$

with

$$A^{MT}_{mnij} = [I_{ijmn} - (1 - z)T^{II}_{ijkl}(l^M_{klmn} - l^I_{klmn})]^{-1} \tag{21}$$

Consequently, by taking into account the constitutive equations for matrix (12) and inclusion (15), the effective constitutive law is derived as follows:

$$\dot{\Sigma}_{ij} = z\dot{\sigma^I_{ij}} + (1 - z)\dot{\sigma^M_{ij}} = L^{eff}_{ijmn}\dot{E}_{mn} - M^{eff}_{ij}\dot{T} \tag{22}$$

ACCEPTED MANUSCRIPT

with

$$\begin{aligned} L_{ijmn}^{eff} &= z(l_{ijkl}^{I} - l_{ijkl}^{M})A_{klmn}^{MT} + l_{ijmn}^{M} \\ M_{ij}^{eff} &= m_{ij}^{M} + z(c_{ijkl}^{I}\alpha_{kl}^{I} - m_{ij}^{M}) \end{aligned} \tag{23}$$

3. Numerical implementation

In the previous section, it has been shown that local constitutive laws in each phase are required to describe the macro-homogeneous behavior. SMA and elastoplastic subroutines are called upon the overall resolution and returning respective tangent operators. In this part, the numerical implementation of the model is discussed, starting with the implementation of matrix and inclusion behaviors. The non-linear local constitutive equations are solved by an Euler-Implicit scheme using the Newton-Raphson technique. Then the general algorithm taking into account the transition scale is developed.

3.1. Implicit resolution of the SMA matrix constitutive equations

The system is composed of four residual equations unbalanced by two control variables. The Table 1 summarizes the residual equations according to activation case of SMA model: the strain tensor increment $\Delta\varepsilon_{ij}^{M}$ and the temperature increment ΔT. The four residual equations are the transformation residual R_f, the transformation strain residual $R_{\bar{\varepsilon}^T}$, the transformation strain flow residual $R_{\Delta\bar{\varepsilon}_{ij}^{T}}$ and the elastic residual $R_{\sigma_{ij}^{M}}$. Unknown variables are the martensite volume fraction increment Δf, the mean transformation strain increment $\Delta\bar{\varepsilon}_{ij}^{T}$, and the stress tensor increment $\Delta\sigma_{ij}^{M}$. An elastic prediction is defined, followed by some activations tests on transformation and

ACCEPTED MANUSCRIPT

reorientation.

For the transformation activation state, three cases have to be considered: transformation from austenite to martensite, transformation from martensite to austenite or no transformation. The thermodynamics transformation force F_f, presented in the previous section (Eq. 7), is compared with a critical force F_f^{crit}. This critical transformation force depends on material parameters F_f^{max} and F_f^{min}, and takes into account previous loadings (internal loops phenomenon) with memory variables F_f^{mem} and γ_f. The critical force is defined as follows:

$$F_f^{crit} = (1 - \gamma_f)F_f^{min} + \gamma_f F_f^{max} \tag{24}$$

When the transformation is not activated, there is no evolution of martensite volume fraction ($\dot{f} = 0$).

For the reorientation activation state, there are two cases: reorientation or no reorientation. In each case, two residual equations related to the thermodynamic orientation force (Eq. 8) are considered. The first reflects the force intensity, the second reflects the flow direction. When reorientation is activated, the orientation force $F_{\bar{\varepsilon}^T}$ is normalised and takes the same value than $F_{\bar{\varepsilon}^T}^{crit}$, which depends on material parameter $F_{\bar{\varepsilon}^T}^{max}$. The flow direction of mean transformation strain is supposed to be the same as the one of the thermodynamic force $F_{\bar{\varepsilon}^T}$. When reorientation is not activated and the transformation is from austenite to martensite, twinned martensite is formed and macroscopic transformation strain is imposed equal to zero. Otherwise, when reorientation is not activated, the normalised evolution of mean transformation strain is imposed equal to zero.

Whatever the activation state of transformation and reorientation, the elastic

ACCEPTED MANUSCRIPT

residual equation is balanced. This one takes into account every strain contributions (elastic, transformation, orientation, twin accommodation, thermal expansion) and checks the consistence with imposed total strain.

Table 1: Expression of the four residual equations for each mechanism activation cases in SMA matrix constitutive model

Name	phenomenon	activation	expression
R_f	transformation	transformation	$R_f = \left\lvert F_f - [(1-\gamma_f)Ff^{mem}] \right\rvert - F_f^{crit}$
		no transformation	$R_f = \dot{f}$
$R_{\bar{\varepsilon}^T}$	transformation strain	reorientation	$R_{\bar{\varepsilon}^T} = \lvert F_{\varepsilon_{ij}} \rvert_\sigma - F_\varepsilon^{crit}$
		no reorientation, $\dot{f} \leqslant 0$	$R_{\bar{\varepsilon}^T} = \lvert \Delta\bar{\varepsilon}_{ij}^T \rvert = 0$
		no reorientation, $\dot{f} > 0$	$R_{\bar{\varepsilon}^T} = \lvert \Delta(f\bar{\varepsilon}_{ij}^T) \rvert = 0$
$R_{\Delta\bar{\varepsilon}_{ij}^T}$	transformation strain	reorientation	$R_{\Delta\bar{\varepsilon}_{ij}^T} = \lambda_{\bar{\varepsilon}^T} \frac{F_{\varepsilon_{ij}}}{\lvert F_{\varepsilon_{ij}} \rvert_\sigma} - \Delta\bar{\varepsilon}_{ij}^T$
	flow	no reorientation	$R_{\Delta\bar{\varepsilon}_{ij}^T} = \lambda_{\bar{\varepsilon}^T} \frac{\bar{\varepsilon}_{ij}^T}{\lvert \bar{\varepsilon}_{ij}^T \rvert_\varepsilon} - \Delta\bar{\varepsilon}_{ij}^T$
$R_{\sigma_{ij}^M}$	elastic strain	$R_{\sigma_{ij}^M} = (S_{ijmn}^M \sigma_{mn}^M) + \alpha^M \delta_{ij} \Delta T + f\bar{\varepsilon}_{ij}^T + f^{FA}\bar{\varepsilon}_{ij}^{tw} - (\varepsilon_{ij}^M + \Delta\varepsilon_{ij}^M)$	

The evolution of mean twin accommodation strain ($\bar{\varepsilon}_{ij}^{tw}$) is direclty related to the stress field in martensite, and the evolution of twin martensite volume fraction f^{FA} depends on martensite volume fraction and mean twin accommodation strain. Thus, twin accommodation phenomenon is taken into account in the equation system in the elastic strain residual equation $R_{\sigma_{ij}^M}$. The normalisation operators are defined as follows: $|X_{ij}|_\sigma = \sqrt{\frac{3}{2}X_{ij}X_{ij}}$, $|X_{ij}|_\varepsilon = \sqrt{\frac{2}{3}X_{ij}X_{ij}}$ and $|X_{ij}| = \sqrt{X_{ij}X_{ij}}$. $\lambda_{\bar{\varepsilon}^T}$ is the cumulative transformation strain ($\lambda_{\bar{\varepsilon}^T} \geq 0$). All residuals were linearized leading to Jacobian terms which were reversed for each iteration of the Newton-Raphson scheme. Tangent operators are derived from Jacobian inversion during Newton Raph-

ACCEPTED MANUSCRIPT

son process. More details about matrix model and numerical scheme can be obtained in Chemisky (2009) and Duval (2009).

3.2. Implicit resolution of the elastoplastic inclusion

The system is composed of two residual equations unbalanced by two control variables: the strain tensor increment $\Delta\varepsilon^I_{ij}$ and the temperature increment ΔT. The Table 2 summarizes the constitutive equations of the elastoplastic model. They are the inclusion elastic residual equation $R_{\sigma^I_{ij}}$ and the inclusion plastic residual equation R_p. Unknown variables are the cumulative plastic strain increment Δp and the stress tensor increment $\Delta\sigma^I_{ij}$. An isotropic elastic prediction is computed, followed by a plastic activation test. The yield condition is checked. If plasticity is not activated, elastic prediction is validated and the variation of cumulative plastic strain Δp is imposed equal to zero. Otherwise, yield surface grows with an isotropic hardening and Δp is computed according to consistency condition. The flow direction is normal to the Mises yield surface.

Table 2: Expression of the two residual equations in elastoplastic constitutive model

Name	phenomenon	activation	expression
$R_{\sigma^I_{ij}}$	elastic strain	$R_{\sigma^I_{ij}} = (S^I_{ijkl}\sigma^I_{kl}) + \alpha^I\delta_{ij}\Delta T + \varepsilon^P_{ij} - (\varepsilon^I_{ij} + \Delta\varepsilon^I_{ij})$	
R_p	plastic strain	activation	$R_p = \lvert\xi_{ij}(\varepsilon^I)\rvert - \sqrt{\frac{2}{3}}K(p) - \sqrt{6}\mu.\Delta p$
		no activation	$R_p = \Delta p$

ξ_{ij} is defined by the following expression: $\xi_{ij}(\varepsilon^I) = 2\mu(dev(\varepsilon^I_{ij} - \varepsilon^P_{ij}))$ and the swift isotropic hardening function is defined by $K(p) = |\sigma^I_{yield}| + H_{iso}p^{\frac{1}{n}}$. μ is the elastic shear modulus of the niobium, which is assumed to have

ACCEPTED MANUSCRIPT

an isotropic and linear elastic behavior. The consistent tangent modulus is calculated according to Simo and Hughes (1998) algorithm.

3.3. Resolution of homogenized system

An Euler-Implicit scheme using the Newton-Raphson technique is also adopted for the scale transition equations as explained in Figure 2.

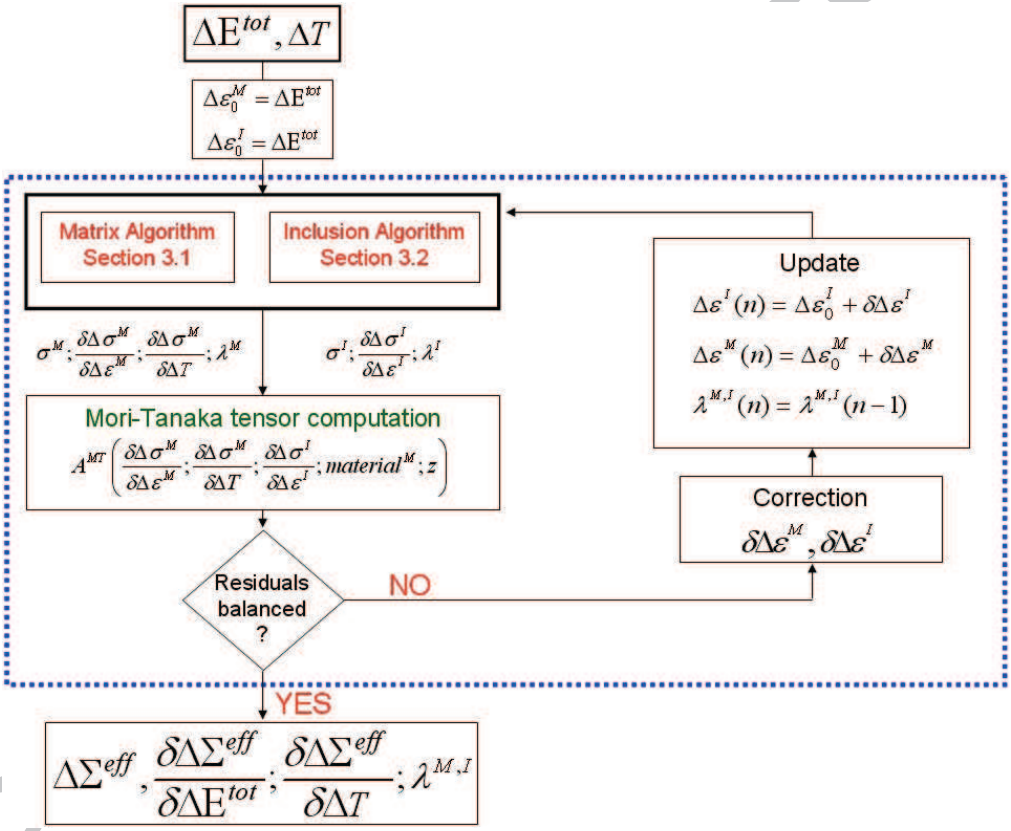

Figure 2: Resolution scheme of global system to model the behavior of NiTi matrix containing elastoplastic inclusions with Mori-Tanaka scale transition technique

Initial value of strain increment inside each phase is assumed to be equal

ACCEPTED MANUSCRIPT

to the effective strain increment ($\Delta\varepsilon_0^M = \Delta\varepsilon_0^I = \Delta E^{tot}$). Temperature is assumed to be homogeneous in the RVE. Strain increments inside matrix and inclusion unbalance their respective system ("Matrix Algorithm" and "Inclusion Algorithm" in Figure 2, respectively), and the corresponding tangent operators and internal variables values (λ) are computed. A first approximation of the Mori-Tanaka tensor is also computed, and two equations have to be balanced:

$$\begin{aligned} \Delta\varepsilon_{ij}^I &= A_{ijkl}^{MT}\Delta\varepsilon_{kl}^{tot} \\ \Delta\varepsilon_{ij}^M &= \frac{1}{1-z}\Big((I_{ijkl} - zA_{ijkl}^{MT})\Delta\varepsilon_{kl}^{tot}\Big) \end{aligned} \tag{25}$$

If these equations are not balanced, corrections are added to strain increment inside each phase through Newton Raphson scheme. Once equilibrium is obtained into each phase, the Mori-Tanaka tensor is updated taking into account new values of matrix and inclusion tangent operators. Thus, the coherence between strains prediction and the computed strains depending on Mori-Tanaka tensor is checked, by balancing the residual equations presented in Table 3. If they are unbalanced, the strain into each phase is corrected by Newton Raphson algorithm.

Table 3: Residual equations related to the homogenisation strategy

Name	associated variable	expression
$R_{\Delta\varepsilon_{ij}^I}$	inclusion strain increment	$R_{\Delta\varepsilon_{ij}^I} = \Delta\varepsilon_{ij}^I - A_{ijkl}^{MT}\Delta\varepsilon_{kl}^{tot}$
$R_{\Delta\varepsilon_{ij}^M}$	matrix strain increment	$R_{\Delta\varepsilon_{ij}^M} = \Delta\varepsilon_{ij}^M - \frac{1}{1-z}\Big((I_{ijkl} - zA_{ijkl}^{MT})\Delta\varepsilon_{kl}^{tot}\Big)$

ACCEPTED MANUSCRIPT

3.4. $Ni_{47}Ti_{44}Nb_9$ material parameters identification

The proposed model involves twenty material parameters: thirteen related to the matrix SMA model, six to the inclusion elastoplastic model and one to the Mori-Tanaka transition scale (Table 4). Some of these parameters are identified thanks to experimental tests on $Ni_{47}Ti_{44}Nb_9$ conducted by authors, others from experimental tests on $Ni_{47}Ti_{44}Nb_9$ presented in literature, and others with experimental tests on $Ni_{51}Ti_{49}$ (a composition close to the NiTi matrix composition). An important part of experimental results on $Ni_{47}Ti_{44}Nb_9$ issued from literature can not be exploited, due to predeformation: as described in section 1, $Ni_{47}Ti_{44}Nb_9$ behavior is strongly influenced by predeformation, which is unknown on studied samples. Thus, several parameter values given in literature are not adapted. Moreover, the complexity of the microstructure and the low martensitic transformation temperature imply that some parameters are not easily identifiable by testing. They have to be then estimated, based on a NiTi whose composition is close to $Ni_{51}Ti_{49}$ for the matrix.

Parameters experimentally identified are Young modulus, volume fraction of inclusions and transformation temperatures. Despite of obtained experimental results by nanoindentation, showing a weak elastic anisotropy, the elastic behavior of the NiTi matrix was assumed to be isotropic with a Young modulus E^M of 80 GPa. Regarding the transformation temperatures, the following values were obtained by classical DSC tests: M_s = -101 °C and M_f = -151 °C, and A_s = 59 °C and A_f = 63 °C for a predeformed sample. Parameters issued from literature are the effective thermal expansion coefficient ($\alpha^{eff} = \alpha^M = \alpha^I$) and the critical orientation stress ($F^{max}_{\bar{\varepsilon}^T}$). Thermal ex-

ACCEPTED MANUSCRIPT

pansion is assumed identical in both matrix and inclusions, and constant with temperature. It was identified by He et al. (2006) to $\alpha = 8$ μm/(m.C) at 20 °C. Maximum variants stress orientation F_{ε}^{max} has been identified to 125 MPa by Xiao et al. (2007) with tensile tests at -70 °C on recrystallized $Ni_{47}Ti_{44}Nb_9$. Among the parameters of the matrix material, two are strongly related to predeformation: the maximum transformation strain in tension and the b parameter giving transformation temperatures evolution with stress. Indeed, predeformation induces plastic strain into inclusions, but also into matrix with the consequence of reducing the maximal transformation strain. Wang et al. (2008) have studied superelastic NiTi with a tension maximal transformation strain of 5.5 %. After applying a deformation of 12 %, the tension transformation strain decreases to 2.5%. DSC predeformed samples study revealed that the predeformation in the $Ni_{47}Ti_{44}Nb_9$ studied in this work is close to 14 %, according to He and Rong (2004). Thus, the maximal transformation strain in tension adopted for simulation of $Ni_{47}Ti_{44}Nb_9$ is 2%. Compressive tests are not conducted, and maximal transformation strain in compression is adopted by assuming no evolution in asymmetry during predeformation. The maximal transformation strain in compression is thereby 1.6%. Similarly, b material parameter is directly related to the phase transformation entropy variation B and to the maximal transformation strain ε_{max}^{T} by the relation $B = b\varepsilon_{max}^{T}$. However, it also depends on the imposed material predeformation. Liu et al. (2006) have studied the influence of cycling on the maximal transformation strain and on b parameter. They showed that in the case of the reverse transformation, the b value is inversely proportional to the maximal transformation strain. In a NiTi sam-

ACCEPTED MANUSCRIPT

ple with initial maximal transformation strain of 4.3%, this strain decreases to 3.8% and 3% for respectively 5 and 117 cycles. The parameter b increases with the number of cycles, respectively to 6.75 MPa/°C, 7 MPa/°C and 7.65 MPa/°C. By extrapolation, the adopted b parameter is 10 MPa/°C in order to be consistent with the maximal transformation strain adopted value. The incompatibility parameters H_f, H_ε and H_{twin} are uneasy to identify on macroscopic tests because they are disturbed by niobium inclusions. They are extrapolated to their values for a $Ni_{51}Ti_{49}$ alloy and are respectively equal to 5 MPa, 2.1 GPa and 40 GPa. Internal loop parameter r_f is fixed to 0.7. Material parameters for niobium are obtained by identification and comparison with experimental results in Nemat-Nasser and Guo (2000). They have studied the behavior of pure niobium by tensile tests. Finally, inclusion volume fraction is obtained by SEM observations and fixed to 0.1. Table 4 summarizes the identified parameter values.

4. Results and discussion

The model has been implemented in the commercial Finite Element Code ABAQUS®, via the User MATerial UMAT subroutine. Numerical simulations, for various loadings, based on the developed model are presented in this section. Elastoplastic inclusions induce many various effects on effective memory behavior. Although the aim of this paper is to study the $Ni_{47}Ti_{44}Nb_9$ behavior, simple cases considering only elastic inclusions are firstly presented. They permit to improve understanding of inclusion stiffness effect on SMA matrix behavior. In this part, simulations are conducted with material parameters different from those listed in Table 4 and chosen to avoid plastic

ACCEPTED MANUSCRIPT

Table 4: Material parameter for predeformed $Ni_{47}Ti_{44}Nb_9$ simulation

Parameter	Unit	Description	Value	Origin
E^M	MPa	SMA Young modulus	80000	Nanoindentation
ν^M	-	SMA Poisson ratio	0.3	$Ni_{51}Ti_{49}$
α^M	μm/(m°C)	Thermal expansion coefficient	8	(He et al., 2006)
ε^T_{trac}	-	Maximal transformation strain in tension	0.02	$Ni_{51}Ti_{49}$
ε^T_{comp}	-	Maximal transformation strain in compression	0.016	$Ni_{51}Ti_{49}$
b	MPa/°C	Transformation temperatures variation with stress	10	(Liu et al., 2006)
M_s	°C	Martensite start temperature	-101	DSC
A_f	°C	Austenite finish temperature	63	DSC
r_f	-	Internal loop parameter	0.7	$Ni_{51}Ti_{49}$
$F^{max}_{\bar{\varepsilon}^T}$	MPa	Critical reorientation stress	125	(Xiao et al., 2007)
H_f	MPa	Transformation interaction parameter	5	$Ni_{51}Ti_{49}$
H_ε	MPa	Orientation interaction parameter	2100	$Ni_{51}Ti_{49}$
H_{twin}	MPa	Twin accommodation parameter	40000	$Ni_{51}Ti_{49}$
E^I	MPa	Inclusion Young modulus	53000	Identification
ν^I	-	Inclusion Poisson ratio	0.3	Identification
α^I	μm/(mC)	Thermal expansion coefficient	8	(He et al., 2006)
σ^Y	MPa	Inclusion plastic yield stress	70	Identification
H^{iso}	MPa	Plastic hardening parameter	450	Identification
n	-	Plastic hardening parameter	4	Identification
z	-	Inclusion volume fraction	0.1	SEM

strain into inclusions. Then, results with elastoplastic inclusions describing the $Ni_{47}Ti_{44}Nb_9$ behavior are discussed. Material parameters are those identified in the previous section and the martensite stabilization is studied. Eventually, the tightening application considering the recovery stress property is simulated and obtained results with NiTi and NiTiNb are compared. The aim of this section is to highlight the general influence of elastic-plastic

ACCEPTED MANUSCRIPT

inclusion addition in SMA matrix, and to apply this to NiTiNb case. There are no developments on the validation of the model by comparisons with experimental tests. A complete experimental study has been realized on a device instrumented with strain gauges containing a NiTiNb ring, on which the present model has been validated by Finite Element Modeling in various geometrical configurations (Piotrowski et al., 2012).

4.1. Elastic inclusions

In this section, inclusion stiffness influence on the effective superelastic behavior is studied. Isotropic elastic inclusions in NiTi SMA matrix are considered. Two kinds of elastic inclusions are considered. In one case, the inclusion's Young modulus is greater than the matrix one (E=140 GPa). In the second case, it is smaller (E=10 GPa). Five values of volume fraction of inclusions are considered (z = 0.001, 0.05, 0.1, 0.15 and 0.2). Material parameters of modeled alloy are listed in Table 5. A compressive load at 60 °C is simulated for an homogeneous stress-strain state, until a stress level of 700 MPa. It is followed by a full unloading. In each case, the effective longitudinal stress evolution with effective longitudinal strain is represented. Figures 3a) and 4a) represent the effective behavior computed, with Young modulus E^I of 140 and 10 GPa, respectively. In each case, the matrix behavior is shown for $E^I = 140$ GPa (Figure 3b) and for $E^I = 10$ GPa (Figure 4b). In the first case, inclusions make the effective behavior more stiff: the bigger is the volume fraction, the stiffer is the effective behavior. Moreover, it can be seen that whatever the inclusion volume fraction, stiff inclusions do not affect the critical stress of martensitic transformation. In fact, Figure 3 shows that the phase transformation occurs in the matrix starting from the

ACCEPTED MANUSCRIPT

Table 5: Material parameter values adopted to simulate a NiTi with two kinds of elastic inclusions and fives values of volume fraction of inclusions

Parameter	Unit	Description	Value
E^M	GPa	SMA Young modulus	70
ν^M	-	SMA Poisson ratio	0.3
α^M	μm/(m°C)	Thermal expansion coefficient	8
ε^T_{trac}	-	Maximal transformation strain in tension	0.05
ε^T_{comp}	-	Maximal transformation strain in compression	0.04
b	MPa/°C	Transformation temperatures variation with stress	5
M_s	°C	Martensite start temperature	20
A_f	°C	Austenite finish temperature	50
r_f	-	Internal loop parameter	0.6
$F^{max}_{\bar{\varepsilon}^T}$	MPa	Critical reorientation stress	160
H_f	MPa	Transformation interaction parameter	4
H_ε	GPa	Orientation interaction parameter	10
H_{twin}	GPa	Twin accommodation parameter	40
E^I	GPa	Inclusion Young modulus	140 ; 10
ν^I	-	Inclusion Poisson ratio	0.3
α^I	μm/(m°C)	Thermal expansion coefficient	8
z	-	Inclusion volume fraction	0.001 ; 0.05 ; 0.1 ; 0.15 ; 0.2

same stress level about 400 MPa for any volume fraction of inclusion. This could be explained by the fact that the inclusions, because of their high stiffness, present rigid body behavior that induce a very weak influence on the matrix behavior. In the second case, the Figure 4 shows that the effective critical transformation stress is related to the fraction of inclusion: when the fraction of compliant inclusion is higher, the effective critical stress of transformation is lower. Consequently, it is possible to decrease the effective critical stress of a shape memory alloy by adding some compliant inclusions.

ACCEPTED MANUSCRIPT

Once the martensite transformation starts, the effective behavior is similar whatever the volume fraction of soft inclusions. Simulations with inclusion fraction of 0.001 can be considered as ones without inclusions. In these cases, it was verified that the matrix behavior is the same as the effective one.

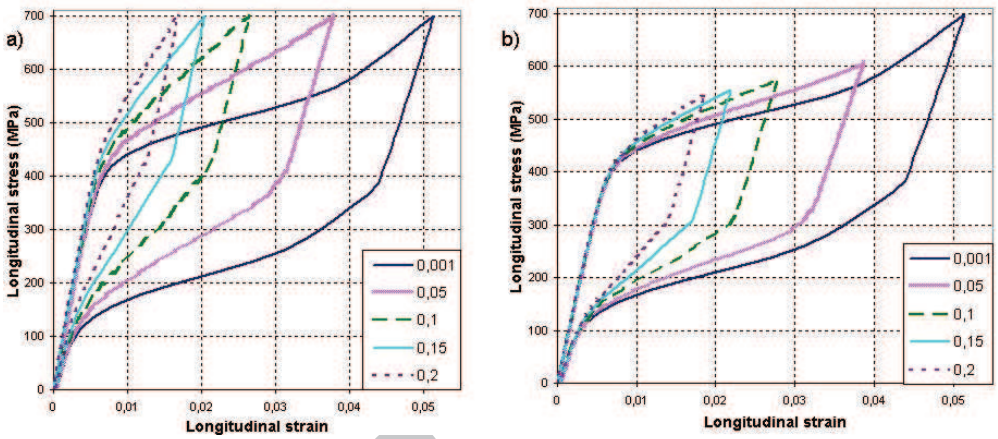

Figure 3: Modeling of NiTi matrix with stiff elastic inclusions ($E^I = 140$ GPa) - a) effective behavior; b) matrix behavior

ACCEPTED MANUSCRIPT

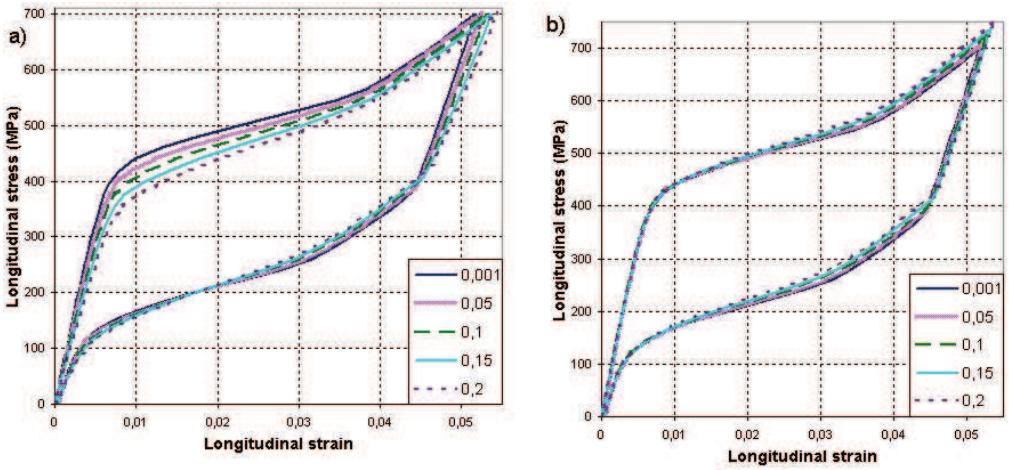

Figure 4: Modeling of NiTi matrix with soft elastic inclusions ($E^I = 10$ GPa) - a) effective behavior; b) matrix behavior

Three variables evolutions are studied: the evolution of martensite volume fraction with inclusion volume fraction at 700 MPa, the width of stress hysteresis and the maximal transformation strain evolution with inclusion volume fraction. It can be seen in Figure 5 that the transformation strain at 700 MPa is strongly influenced by rigid inclusions. Whereas the maximal transformation strain without inclusion is about 3.6 %, a decrease until 2.1 % is observed with 20 % of rigid inclusions. In the case of compliant inclusions, the total strain is a little higher when the fraction of inclusions increases, but they have no influence on transformation strain at 700 MPa. In these cases, the martensitic transformation is conducted until saturation. This point is confirmed by the Figure 6 which highlights the evolution of martensite volume fraction with inclusion volume fraction. It can be seen that the alloy is fully martensitic at 700 MPa for each value of compliant inclusions. With

ACCEPTED MANUSCRIPT

stiff inclusions, the martensitic transformation is not completed at 700 MPa: there is 70 % of martensite with 10 % of inclusions and only 43 % with 20 % of inclusions.

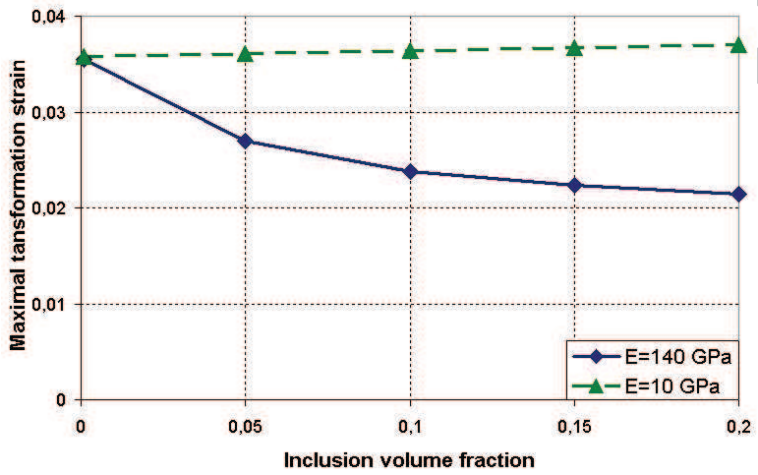

Figure 5: Evolution of maximal transformation strain with inclusion volume fraction at stress level of 700 MPa

ACCEPTED MANUSCRIPT

ACCEPTED MANUSCRIPT

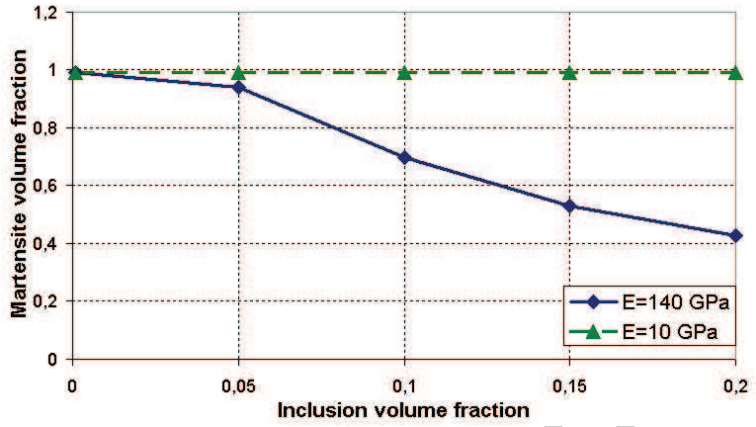

Figure 6: Evolution of martensite volume fraction with inclusion volume fraction at stress level of 700 MPa

Moreover, it can be seen that the width of stress hysteresis decreases when the fraction of inclusion increases. The Figure 7 shows that the hysteresis, whose width is around 275 MPa without inclusions, decreases until 200 MPa in stiff inclusions case, and 225 MPa in compliant inclusions case.

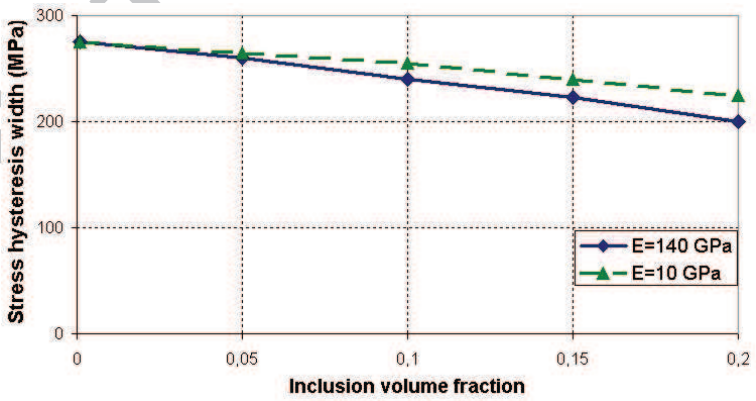

Figure 7: Evolution of the width of the stress hysteresis with inclusion volume fraction

ACCEPTED MANUSCRIPT

In order to study inclusions influence on macroscopic behavior in reorientation cases, compressive loads have been simulated with elastic inclusions at temperature lower than M_f. Similar results to the superelastic case have been obtained, concerning maximal transformation strain evolution and hysteresis size with the fraction of inclusions. They are not detailed here, elastoplastic inclusions are considered in next section.

4.2. Elastoplastic inclusions in $Ni_{47}Ti_{44}Nb_9$: influence on A_s temperature

In this section, simulations with $Ni_{47}Ti_{44}Nb_9$ are conducted in order to study elastoplastic inclusions impact on effective thermo-mechanical behavior. In particular, the mechanism of A_s temperature increase is highlighted. Comparisons are made between $Ni_{47}Ti_{44}Nb_9$, an equivalent alloy with 25 % of niobium inclusion instead of 10 %, and an equivalent alloy with 10 % of brittle inclusions ($\sigma^Y = 400$ MPa et $H^{iso} = 70$ MPa) instead of ductile inclusions. These comparisons permit to understand the influence of elastoplastic inclusion volume fraction, and the influence of hardening properties.
According to material parameter identification section, some material parameters are strongly related to the predeformation: transformation temperature (He and Rong, 2004), maximal transformation strain and b parameter. Since the aim of this part is to study A_s temperature increase with predeformation, $Ni_{47}Ti_{44}Nb_9$ material parameters values are considered without predeformation. That means M_s = -57 °C, A_f = 5 °C, $\varepsilon^T_{trac} = 0.05$, $\varepsilon^T_{comp} = 0.04$ and $b = 3$ MPa/°C.

Simulations are conducted for an homogeneous stress-strain state. The material, initially austenitic, is cooled from 100 °C to -70 °C to induce twinned

ACCEPTED MANUSCRIPT

martensite formation. A stress loading of 700 MPa is applied leading to martensitic orientation and plastic strain, respectively in matrix and inclusions. The pressure is then fully relaxed. After having locked the strain value, the material is heated in order to activate the reverse transformation and induce stress increase.

The applied stress induces a strain between 7 and 8 %. Figure 8 shows

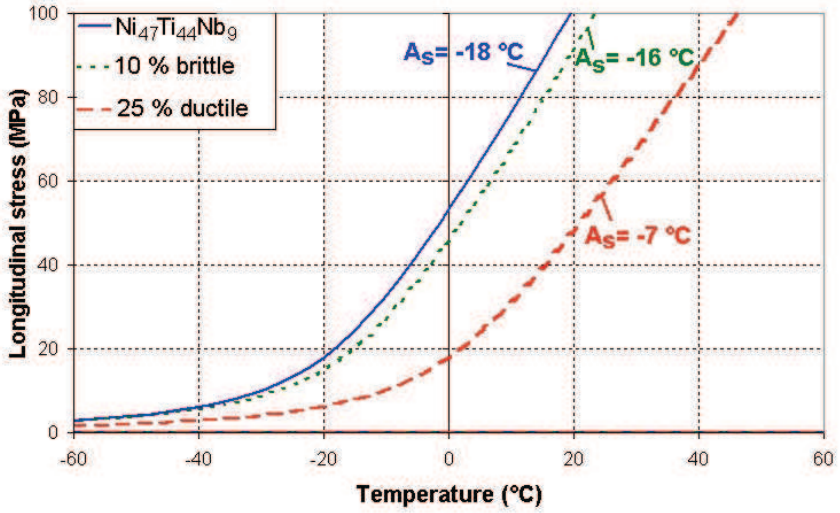

Figure 8: Stress-Temperature diagram for three NiTiNb alloys after the same predeformation. A_s temperature evolution by predeformation - Comparison between $Ni_{47}Ti_{44}Nb_9$ (ductile inclusions) and two composites having identical matrix properties, the first with 10 % of brittle inclusions and the second with 25 % of ductile inclusions

that the model takes into account the predeformation impact on A_s reverse transformation temperature. Indeed, the plastic strain due to predeformation in inclusions modifies the reverse transformation temperature. Without predeformation, the A_s temperature of $Ni_{47}Ti_{44}Nb_9$ is -23 °C whereas the value after is -18 °C in $Ni_{47}Ti_{44}Nb_9$ case, -16 °C in case with brittle inclu-

ACCEPTED MANUSCRIPT

sions and -7 °C in the case with 25 % of ductile inclusions. The influence of inclusions behavior on predeformation is due to the inclusion ability to exhibit plastic strain at low stress. To understand the phenomenon, Figure 9 shows the stress evolution with strain of $Ni_{47}Ti_{44}Nb_9$ into each phase, for ductile (a) and brittle (b) inclusions, and in a NiTiNb with 25 % of inclusions.

ACCEPTED MANUSCRIPT

ACCEPTED MANUSCRIPT

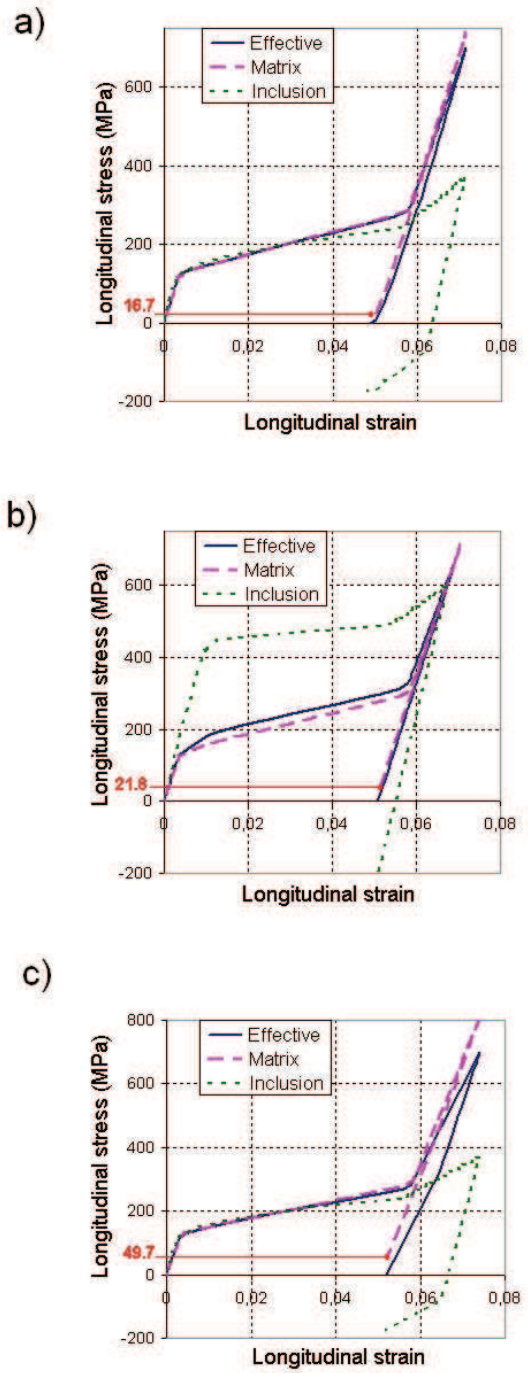

Figure 9: Effective stress evolution into each phase during predeformation - Comparison of $Ni_{47}Ti_{44}Nb_9$ (a) with two composites having identical matrix properties, the first one contains 10 % of brittle inclusions (b) and the second one 25 % of ductile inclusions (c)

ACCEPTED MANUSCRIPT

Martensite stabilization phenomenon can be explained by focusing on the SMA matrix behavior. In the first case, the residual stress in the matrix after predeformation is about 16.7 MPa, whereas it is about 21.8 MPa in the second one and 49.7 MPa in the third. During the heating, the internal stress delays the beginning of the reverse transformation, as illustrated on Figure 10 which shows the behavior in the matrix during predeformation followed by heating.

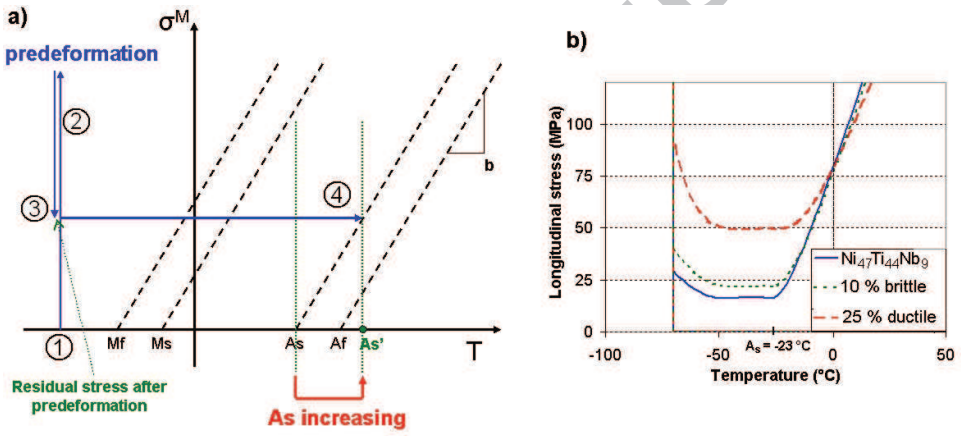

Figure 10: a) A_s temperature increase explanation: non zero stress state in SMA matrix shifts reverse transformation toward higher temperature - b) illustration with comparison between $Ni_{47}Ti_{44}Nb_9$, NiTi Matrix with 10 % of brittle inclusions and NiTi matrix with 25 % of ductile inclusions

1. Before the predeformation which is applied in twinned martensite state, there is no effective stress, each phase is in a non-stress state.
2. When predeformation is applied, the stress increases in matrix
3. After the relaxation of predeformation, the effective stress turns to zero.

ACCEPTED MANUSCRIPT

However, a residual stress σ_{res}^{M} remains in the matrix as shown in Figure 9

4. Shape memory alloy transformation temperatures depend on stress level within b parameter, and the effective shape memory effect of $Ni_{47}Ti_{44}Nb_9$ is directly related to shape memory matrix. During heating, the reverse transformation occurs when the temperature T becomes greater than $(A_s + \sigma_{res}^{M}/b)$. There is a compressive stress state in inclusions.

The difference of 33 MPa between NiTiNb with 9 and 25 % of ductile inclusions should induce a difference of A_s about 11 °C with $b = 3$ MPa/°C. This is obtained from the model. Consequently, the presented model is able to predict the reverse transformation temperature evolution induced by plastic strain in inclusions.

However, this prediction is only qualitative. Experimental results from He and Rong (2004) give an A_s increase around 50 °C for a $Ni_{47}Ti_{44}Nb_9$ predeformed at 8.4 % which is higher than the 11 °C predicted by the model. At this level, the stress in the SMA matrix is greater than the NiTi plastic yield stress, and the plastic strain that should occurs in the matrix modify the value of internal remaining stress in SMA. Plastic behavior of shape memory matrix should be considered in order to accuratly simulate this predeformation above 8%. This result is interesting to improve knowledge of martensite stabilization into $Ni_{47}Ti_{44}Nb_9$. Nevertheless, even if this model is not able to predict quantitatively the predeformation, it is able to simulate the thermomechanical behavior of predeformed $Ni_{47}Ti_{44}Nb_9$. In industrial applications, $Ni_{47}Ti_{44}Nb_9$ components are usually delivered in the predeformed state. Con-

ACCEPTED MANUSCRIPT

sequently, this model can be used as design tool for industrial applications.

4.3. Tightening application: comparison between NiTi and $Ni_{47}Ti_{44}Nb_9$

The studied device consists of a SMA ring which tightens on an Inconel 825 pipe. Initial internal diameter of the ring is lower than external diameter of the pipe. Initial temperature is 100 °C, well above reverse transformation temperatures of the SMA considered alloy. Ring and pipe dimensions are presented in Table 6. The tightening cycle is the following:

- the SMA ring is cooled to -130 °C, below martensite transformation temperatures,
- the SMA ring is opened by applying a pressure of 150 MPa upon its internal face, the SMA internal diameter becomes greater than pipe external diameter,
- the pressure is relaxed and the Inconel pipe is placed inside the SMA ring,
- the device is heated to 200 °C, above reverse transformation temperatures which induces reverse transformation and tightening,
- the device is cooled until 0 °C.

ACCEPTED MANUSCRIPT

ACCEPTED MANUSCRIPT

Table 6: Dimensions of modeled device

	SMA ring	Elastic pipe
Internal radius (mm)	4	2.56
External radius (mm)	6	4.06
Length (mm)	5	10

Three SMA are studied: NiTi, $Ni_{47}Ti_{44}Nb_9$ with predeformation and $Ni_{47}Ti_{44}Nb_9$ without predeformation. The aim is to highlight niobium influence on macroscopic thermomechanical behavior and the influence of predeformation. NiTi material parameters are those adopted previously (listed in Table 5), and predeformed $Ni_{47}Ti_{44}Nb_9$ ones are listed in Table 4. According to previous section, $Ni_{47}Ti_{44}Nb_9$ without predeformation is obtained by modifying some material parameters from Table 4 (M_s = -57 °C, A_f = 5 °C, ε^T_{trac} = 0.05, ε^T_{comp} = 0.04 and b=3 MPa/°C). Inconel 825 is simulated with an isotropic thermoelastic constitutive law (E = 196,000 MPa, ν = 0.29 and expansion coefficient of 8 μm/(mC)).

An axisymmetric finite element model is considered, with CAX4R (An Abaqus' axisymmetric quadrangular continium element with reduced integration) linear elements. Element size is chosen in order to have 4 elements in ring thickness and a structured discretization. A progressive discretization is adopted for the pipe, in order to have large elements inside the pipe, and small ones outside where contact occurs (same element size in ring and pipe at contact region). A finite sliding frictionless contact, with "hard contact" normal be-

ACCEPTED MANUSCRIPT

havior, is considered. Displacement of both ring and pipe is not allowed in axial direction.

The results of NiTi and predeformed NiTiNb simulations are shown in Figure 11, which represents the equivalent stress level in device at the end of the cycle. For more clarity a 3D representation, obtained by a revolution, is proposed. Although the stress repartition in pipe is the same for NiTi and predeformed $Ni_{47}Ti_{44}Nb_9$, it is greater in the second case with a factor 6.

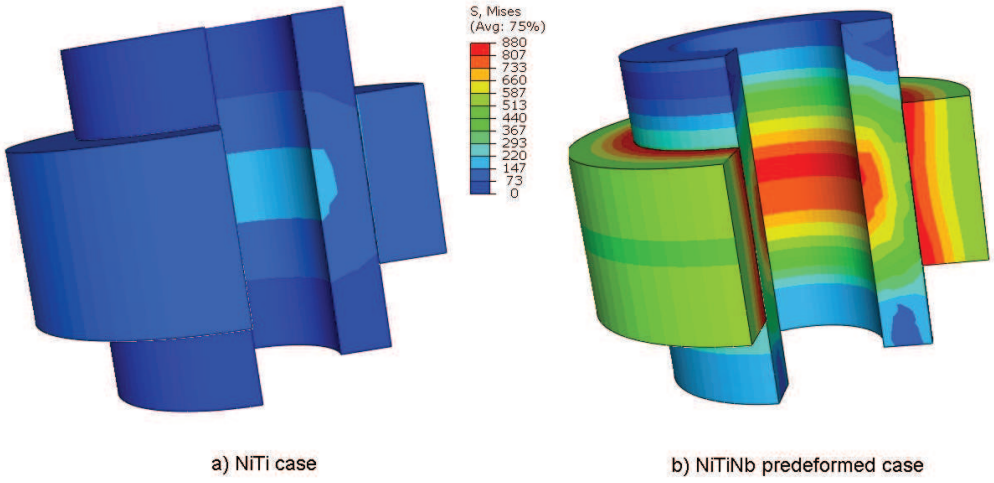

Figure 11: Von Mises equivalent stress (MPa) in NiTi and NiTiNb predeformed ring at the end of applied cycle

Figure 12 shows the contact pressure evolution during heating and cooling steps. It can be seen that during heating, the reverse transformation occurs firstly in $Ni_{47}Ti_{44}Nb_9$ ring around 0 °C, then in NiTi ring at 32 °C and in predeformed $Ni_{47}Ti_{44}Nb_9$ at 53 °C. At 200 °C, the reverse transformation is close to saturation in predeformed $Ni_{47}Ti_{44}Nb_9$ and NiTi cases. The contact pressure is respectively 291 and 284 MPa. However, the reverse transforma-

ACCEPTED MANUSCRIPT

tion is not complete at 200 °C in $Ni_{47}Ti_{44}Nb_9$ case and the contact pressure is only around 212 MPa, as shown in Figure 13. During cooling, the NiTi ring losses contact pressure from 140 °C and there is no contact pressure at 0 °C. This is due to the small hysteresis of the alloy. In $Ni_{47}Ti_{44}Nb_9$, the decrease of contact pressure is smaller but begins at the same temperature. On the contrary, there is no decrease of contact pressure during cooling for predeformed $Ni_{47}Ti_{44}Nb_9$ on a range of 180 °C. The martensitic transformation occurs around 15 °C and the loss of contact pressure is very small.

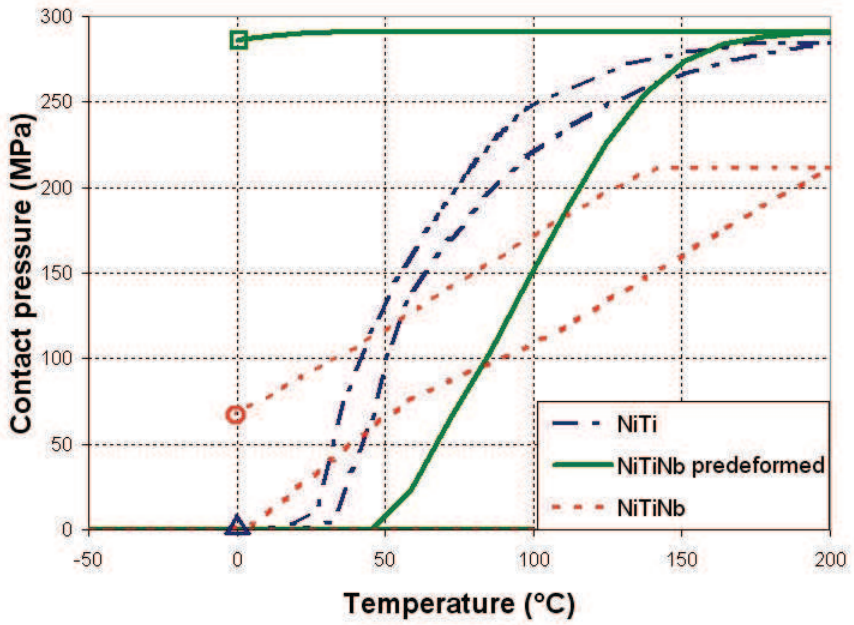

Figure 12: Contact pressure evolution during thermo-mechanical loading - Results on NiTi and NiTiNb with and without predeformation

ACCEPTED MANUSCRIPT

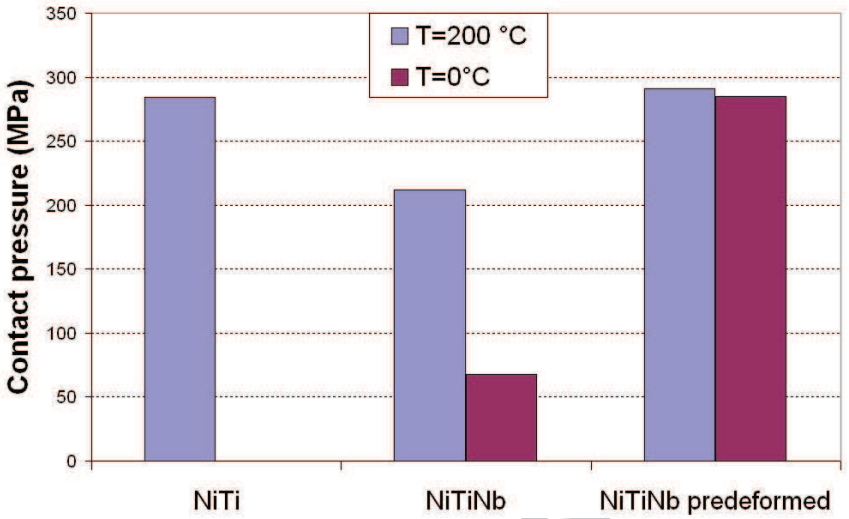

Figure 13: Comparison of contact pressure for NiTi, NiTiNb and predeformed NiTiNb rings - Results at the end of heating (200 °C) and at the end of cycle (0 °C)

5. Conclusion

This paper presents a constitutive model describing the thermo-mechanical behavior of a composite containing elastic or elastoplastic inclusions into a SMA matrix. Inclusions are taken into account by the Mori-Tanaka transition scale. This model has been implemented in the ABAQUS® Finite Element code. The SMA matrix behavior takes into account superelasticity, memory effect and internal loops behavior for complex loading, tension-compression asymmetry and saturations. The inclusions impact on effective behavior is also described (stiffness, elastoplastic behavior, volume fraction of inclusions). Beyond NiTiNb, many kinds of composites could consequently be considered, for example NiTi alloys with Ni_4Ti_3 elastic inclusions and porous shape memory alloys by considering void inclusions.

ACCEPTED MANUSCRIPT

Concerning the $Ni_{47}Ti_{44}Nb_9$ modeling, several tests have been conducted to characterize the alloy and identify model material parameters. The proposed model takes into account the influence of β-Nb spherical inclusions on the effective thermo-mechanical behavior of the alloy. It shows that these inclusions stabilize the martensite after a predeformation, and that they modify the thermo-mechanical behavior of the alloy during mechanical loading until strain of 8%. The stabilization predicted by the model is not as high as experimental values because the internal residual stress induced into SMA matrix during predeformation increases reverse transformation temperature of SMA matrix and consequently the effective behavior. The present model has been validated by experimental/numerical comparisons of a tightening device, using $Ni_{47}Ti_{44}Nb_9$ with a specific predeformation (14%) (Piotrowski et al., 2012). Experimental characterization and extrapolation of literature data have given model material parameters.

Further investigations have to be conducted in order to fully model predeformation phenomenon. The first one is to consider ellipsoidal inclusions, which would be more faithful to the microscopic observations and increases the predicted stabilization. The second one is to take into account the plastic yield stress of the SMA matrix with a model including internal stress induced by predeformation. The third one is to consider little inclusions at a NiTi polycrystal scale and to study inclusions interaction with variants of martensite with a micromechanical approach. This work is in progress (Collard et al., 2008). Moreover, experimental data for tension and torsion tests will be carried out for NiTiNb in order to validate the model prediction of the volume fraction precipitate effect. Finally, the implementation of this model in a fi-

ACCEPTED MANUSCRIPT

nite element code leaded to a design tool for industrial connectic applications.

Acknowledgement - This research has been performed within a project funded by Schlumberger SRPC (Clamart). The authors are grateful to Schlumberger for its financial support. Scientific computing code Simula+ (CEMES/LAMAV/LEMTA/LEM3) has been used in a part of computation.

References

Aoki, T., Shimamoto, A., 2003. Active vibration control of epoxy matrix composite beams with embedded shape memory alloy TiNi fibers. International Journal of Modern Physics B 17, 1744–1749.

Armstrong, W. D., Lorentzen, T., 2001. The self-thermal-plastic response of NiTi shape memory alloy fiber actuated metal matrix composites. International Journal of Solids and Structures 38, 7029–7044.

Auricchio, F., Reali, A., Stefanelli, U., 2007. A three-dimensional model describing stress-induced solid phase transformation with permanent inelasticity. International Journal of Plasticity 23, 207–226.

Bartel, T., Menzel, A., Svendsen, B., 2011. Thermodynamic and relaxation-based modeling of the interaction between martensitic phase transformations and plasticity. Journal of the Mechanics and Physics of Solids 59, 1004–1019.

ACCEPTED MANUSCRIPT

Berveiller, M., Zaoui, A., 1979. An extension of the self-consistent scheme to plastically flowing polycrystals. Journal of the Mechanics and Physics of Solids 26, 325–344.

Bollas, D., Pappas, P., Parthenios, J., Galiotis, C., 2007. Stress generation by shape memory alloy wires embedded in polymer composites. Acta Materialia 55, 5489–5499.

Boudifa, M., Saanouni, K., Chaboche, J., 2009. A micromechanical model for inelastic ductile damage prediction in polycrystalline metals for metal forming. International Journal of Mechanical Sciences 51, 1453–464.

Boyd, J. G., Lagoudas, D. C., 1996. A thermodynamical constitutive model for shape memory materials. Part II. The SMA composite material. International Journal of Plasticity 12, 843–873.

Brinson, L. C., Huang, M. S., Boller, C., Brand, W., 1997. Analysis of controlled beam deflections using SMA wires. Journal of Intelligent Material Systems and Structures 8, 12–25.

Brinson, L. C., Lammering, R., 1993. Finite-element analysis of the behavior of shape-memory alloys and their applications. International Journal of Solids and Structures 30, 3261–3280.

Chemisky, Y., 2009. Modelisation du comportement macroscopique des Alliages a Memoire de Forme - Applications aux materiaux composites. Phd thesis, Metz University.

Chemisky, Y., Duval, A., Patoor, E., Ben Zineb, T., 2011. Constitutive model

ACCEPTED MANUSCRIPT

for shape memory alloys including phase transformation, martensitic reorientation and twins accommodation . Mechanics of Materials 43, 361–376.

Chemisky, Y., Duval, A., Piotrowski, B., Ben Zineb, T., Tahiri, V., Patoor, E., 2009a. Numerical tool for SMA materials simulation - Application to composite structures design. Smart Materials and Structures 1, 1–2.

Chemisky, Y., Piotrowski, B., Ben Zineb, T., Patoor, E., 2009b. Numerical study of mean-field approach capabilities for shape memory alloys matrix composites description. ESOMAT 200903004.

Cherkaoui, M., Berveiller, M., Sabar, H., 1998. Micromechanical modeling of martensitic transformation induced plasticity (TRIP) in austenitic single crystals. International Journal of Plasticity 14, 597–626.

Cherkaoui, M., Sun, Q. P., Song, G., 2000. Micromechanics modeling of composite with ductile matrix and shape memory alloy reinforcement. International Journal of Solids and Structures 37, 1577–1594.

Collard, C., Ben Zineb, T., Patoor, E., Ben Salah, M. O., 2008. Micromechanical analysis of precipitate effects on shape memory alloys behaviour. Materials Science and Engineering A 481-482, 366–370.

Desrumaux, F., Meraghni, F., Benzeggagh, M., 2001. Generalised mori-tanaka scheme to model anisotropic damage using numerical eshelby tensor. Journal of Composite Materials 35, 603–624.

Duval, A., 2009. Modelisation du comportement thermomecanique d'alliages a memoire de forme. Application au dimensionnement de microsystemes et extension en non local. Phd thesis, Nancy University.

ACCEPTED MANUSCRIPT

Entchev, P. B., Lagoudas, D. C., 2002. Modeling porous shape memory alloys using micromechanical averaging techniques. Mechanics of Materials 34, 1–24.

Eshelby, J. D., 1961. Elastic Inclusion and Inhomogeneities. Progress in Solid Mechanics 2, 89.

Feng, X. Q., Sun, Q., 2007. Shakedown analysis of shape memory alloy structures. International Journal of Plasticity 23, 183–206.

Fischer, F. D., Reisner, G., Werner, E., Tanaka, K., Cailletaud, G., Antretter, T., 2000. A new view on transformation induced plasticity (TRIP). International Journal of Plasticity 16, 723–748.

Gao, X., Huang, M., Brinson, L. C., 2000. A multivariant micromechanical model for SMAs Part 1. Crystallographic issues for single crystal model. International Journal of Plasticity 16, 1345–1369.

Goliboroda, I., Rusinko, K., Tanaka, K., 1999. Description of an iron-based shape memory alloy: thermomechanical behavior in terms of the synthetic model. Computational Materials Science 13, 218–226.

Harrison, J. D., Choi, J. Y., Marchant, P. R., 1973. Heat recoverable alloy. United State Patent 3,753,700.

Hartl, D. J., Chatzigeorgiou, G., Lagoudas, D. C., 2010. Three-dimensional modeling and numerical analysis of rate-dependent irrecoverable deformation in shape memory alloys. International Journal of Plasticity 26, 1485–1507.

ACCEPTED MANUSCRIPT

ACCEPTED MANUSCRIPT

He, X. M., Rong, L. J., 2004. DSC analysis of reverse martensitic transformation in deformed Ti-Ni-Nb shape memory alloy. Scripta Materialia 51, 7–11.

He, X. M., Zhao, L. Z., Zhang, S. F., Duo, S. W., Zhang, R. F., 2006. Study of the thermal physical properties of $Ti_{44}Ni_{47}Nb_9$ wide hysteresis shape memory alloys. Materials Science and Engineering A 441, 167–169.

Hill, R., 1965. Continuum micro-mechanisms of elastoplastic polycrystals. Journal of the Mechanics and Physics of Solids 13, 89–101.

Huang, M., Brinson, L. C., 1998. A multivariant model for single crystal shape memory alloy behavior. Journal of the Mechanics and Physics of Solids 46, 1379–1409.

Hutchinson, J. W., 1976. Bounds and self-consistent estimates for creep of polycrystalline materials. Proceedings of the Royal Society London A.

Idesman, A.V., L. V., Stein, E., 2000. Structural changes in elastoplastic material: a unified finite-element approach to phase transformation, twinning and fracture. International Journal of Plasticity 16, 893–949.

Jemal, F., Bouraoui, T., Ben Zineb, T., Patoor, E., Bradai, C., 2009. Modeling of martensitic transformation and plastic slip effects on the thermomechanical behaviour of Fe-based shape memory alloys. Mechanics of Materials 41, 849–856.

Kan, Q., Kang, G., 2010. Constitutive model for uniaxial transformation ratchetting of super-elastic NiTi shape memory alloy at room temperature. International Journal of Plasticity 26, 441–465.

ACCEPTED MANUSCRIPT

Kawai, M., 2000. Effects of matrix inelasticity on the overall hysteretic behavior of TiNi-SMA fiber composites. International Journal of Plasticity 16, 263–282.

Khalil, W., Mikolajczak, A., Bouby, C., Ben Zineb, T., 2012. A constitutive model for Fe-based SMA considering martensitic transformation and plastic sliding coupling: Application to finite element structural analysis. Journal of Intelligent Material Systems and Structures, in Press.

Kouznetsova, V., Geers, M., 2008. A multiscale model of martensitic transformation plasticity. Mechanics of Materials 40, 641–657.

Kroner, E., 1961. Zur plastischen verformung des vielkristalls. Acta Metall. 9, 155–161.

Levitas, V., 2002. Critical thought experiment to choose the driving force for interface propagation in inelastic materials . International Journal of Plasticity 18 (11), 1499–1525.

Liu, Y., Mahmud, A., Kursawe, F., Nam, T. H., 2006. Effect of pseudoelastic cycling on the Clausius-Clapeyron relation for stress-induced martensitic transformation in NiTi. Journal of Alloys and Compounds 449, 82–87.

Lu, Z. K., Weng, G. J., 2000. A two-level micromechanical theory for a shape-memory alloy reinforced composite. International Journal of Plasticity 16, 1289–1307.

Meraghni, F., Benzeggagh, M., 1995. Micromechanical modelling of matrix degradation in randomly oriented discontinous-fibre composites. Composites Science and Technology 55, 171–186.

ACCEPTED MANUSCRIPT

Mercier, S., Molinari, A., 2009. Homogenization of elastic-viscoplastic heterogeneous materials: Self-consistent and Mori-Tanaka schemes. International Journal of Plasticity 25, 1024–1048.

Mori, T., Tanaka, K., 1973. Average stress in matrix and average elastic energy of materials with misfitting inclusions. Acta Metallurgica 21, 571–574.

Muller, C., Bruhns, O. T., 2006. A thermodynamic finite strain model for pseudoelastic shape memory alloys. International Journal of Plasticity 22, 1658–1682.

Nam, 1990. Japan Institute of Metals 11 31, 959–967.

Nemat-Nasser, S., Guo, W. G., 2000. Flow stress of commercially pure niobium over a broad range of temperatures and strain rates. Materials Science and Engineering A 284, 202–210.

Oh, J. T., Park, H. C., Hwang, W., 2001. Active shape control of a double-plate structures using piezoceramics and SMA wires. Smart Materials and Structures 10, 1100–1106.

Panico, M., Brinson, L. C., 2007. A three-dimensional phenomenological model for martensite reorientation in shape memory alloys. Journal of the Mechanics and Physics of Solids 55, 2491–2511.

Panico, M., Brinson, L. C., 2008. Computational modeling of porous shape memory alloys. International Journal of Solids and Structures 45, 5613–5626.

ACCEPTED MANUSCRIPT

Patoor, E., Eberhardt, A., Berveiller, M., 1996. Micromechanical modelling of superelasticity in shape memory alloys. Journal De Physique. IV JP 6 (1), C1–277–C1–292.

Patoor, E., Lagoudas, D. C., Entchev, P. B., Brinson, L. C., Gao, X., 2006. Shape memory alloys, part i: general properties and modeling of single crystals. Mechanics of Materials 38, 391–429.

Peng, X., Pi, W., Fan, J., 2008. A microstructure-based constitutive model for the pseudoelastic behavior of NiTi SMAs. International Journal of Plasticity 24, 966–990.

Petit, B., Gey, N., Cherkaoui, M., Bolle, B., Humbert, M., 2007. Deformation behavior and microstructure/texture evolution of an annealed 304 AISI stainless steel sheet. Experimental and micromechanical modeling. International Journal of Plasticity 23, 323–341.

Peultier, B., Ben Zineb, T., Patoor, E., 2006. Macroscopic constitutive law of shape memory alloy thermomechanical behaviour. Application to structure computation by FEM. Mechanics of Materials 38, 510–524.

Piao, M., Otsuka, K., Miyazaki, S., Horikawa, H., 1993. Mechanism of the As temperature increase by pre-deformation in thermoelastic alloys. Materials Transactions, JIM 34, 919–929.

Piotrowski, B., Ben Zineb, T., Patoor, E., Eberhardt, A., 2012. A finite-element based numerical tool for $Ni_{47}Ti_{44}Nb_9$ SMA structures design: application to tightening rings. Journal of Intelligent Material Systems and Structures 23, 141–153.

ACCEPTED MANUSCRIPT

Popov, P., Lagoudas, D. C., 2007. A three-dimensional constitutive model for shape memory alloys incorporating pseudoelasticity and detwinning of self-accommodated martensite. International Journal of Plasticity 23, 1679–1720.

Simo, J. C., Hughes, T. J. R., 1998. Computational Inelasticity. Springer-Verlag, Berlin.

Strnadel, B., Ohashi, S., Ohtsuka, H., Miyazaki, S., Ishihara, T., 1995. Effect of mechanical cycling on the pseudoelasticity characteristics of Ti-Ni and Ti-Ni-Cu alloys. Material Science and Engineering A 203, 187–196.

Thiebaud, F., Lexcellent, C., Collet, M., Foltete, E., 2007. Implementation of a model taking into account the asymmetry between tension and compression, the temperature effects in a finite element code for shape memory alloys structures calculations. Computational Materials Science 41, 208–221.

Wang, X., Xu, B., Yeu, Z., 2008. Phase transformation behavior of pseudoelastic NiTi shape memory alloys under large strain. Journal of Alloys and Compounds 463, 417–422.

Wilkins, M. L., 1964. Calculation of Elastic-Plastic Flow. B. Adler et al., eds, Methods of Computational Physics, Academic Press, New York.

Xiao, F., Ma, G., Zhao, X., Xu, H., Jiang, H., Rong, L., 2007. A novel TiNiNb shape memory alloy with high yield strength and high damping capacity. International Conference on Smart Materials and Nanotechnology in Engineering,Proc. SPIE 6423, 64232L.

ACCEPTED MANUSCRIPT

ACCEPTED MANUSCRIPT

Zaki, W., Moumni, Z., 2007. A three-dimensional model of the thermomechanical behavior of shape memory alloys. Journal of the Mechanics and Physics of Solids 55, 2455–2490.

Zhang, C. S., Wang, Y. Q., Chai, W., Zhao, L. C., 1991. The study of constitutional phases in a $Ni_{47}Ti_{44}Nb_9$ shape memory alloy. Materials Chemistry and Physics 28, 43–50.

Zhang, C. S., Zhao, L. C., Duerig, T. W., Wayman, C. M., 1990. Effects of deformation on the transformation hysteresis and shape memory effect in a $Ni_{47}Ti_{44}Nb_9$ alloy. Scripta Metallurgica et Materialia 24, 1807–1812.

Zhang, R. X., Ni, Q. Q., Natsuki, T., Iwamoto, M., 2007. Mechanical properties of composites filled with SMA particles and short fibers. Composite Structures 79, 90–96.

Zhao, L. C., Duerig, T. W., Justi, S., Melton, K., Proft, J. L. Y., 1990. The study niobium rich precipitates Ni Ti Nb shape memory alloy. Scripta metallurgica 24, 221–225.

ACCEPTED MANUSCRIPT